Anti-aliasing Filter for Coherent Airborne Radar

Bachelor's Thesis

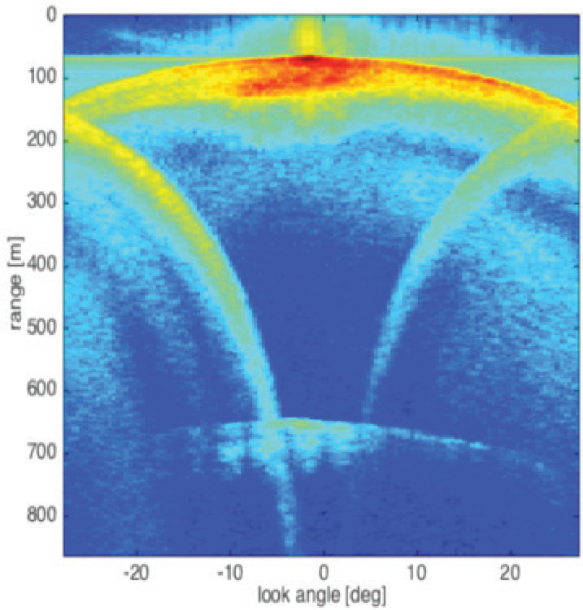

Nick Pettha Thanthrige
June 2017

Supervisor:
Jørgen Dall

DTU Space
National Space Institute

Preface

This bachelor thesis is written in partial fulfillment of a bachelor degree in Electrical Engineering at the Technical university of Denmark, DTU Space. This thesis was carried out in the period February 2017 to June 2017, and is equivalent to a workload of 15 ECTS points. The report describes the design and test of filters for the nadir looking radar POLARIS.

Abstract

The Technical University of Denmark has developed a P-band ice sounding radar (POLARIS). The radar is a nadir looking pulse radar that emits pulses of long duration. The signal returning to radar is masked by surface clutter and thermal noise, which are unwanted components in the radar system.

This thesis deals with the examination of these noise artifacts, and anti-aliasing filters are designed for several scenarios. It was found that signal returns for propegation in warm ice is heavily masked by clutter arising from the surface of the ice sheet, and therefore it is hard to suppress. This stands in contrast to cold ice, where high signal-to-clutter ratios are obtained. It is found that the bedrock exhibits a strong return, and can in most cases easily be detected.

Acknowledgements

I would like to thank my supervisor Jørgen Dall, for a good project period, great advice and for leading one in the right direction by asking the right questions. I would also like to thank Markus Henriksen and Peter Karstensen, fellow bachelor students, for being able to study with you throughout the semester. At last i would like to thank Jacob Ahl for constructive radar theory discussions in the last stages of the project.

Contents

List of Figures

List of Tables

CHAPTER 1

Introduction

Low frequency radars are used to measure below the surface of ice sheets. The coherent airborne radar POLARIS[1] developed at DTU [6] is an ice sounder that operates above the Greenland ice sheet. Ice sounders and other airborne ground penetrating radars are used to study the subsurface of the earth, and plays a major role in todays earth science. The transmitted radar signal has a bandwidth that depends on flight speed and the resolution in the flight direction. The sampling frequency is much higher than the signal bandwidth, it equals the pulse repetion frequency (PRF) of the radar and thereby the signal is oversampled. By oversampling greater than the Nyquist rate[2], lowpass filtering and decimation, a high signal to noise ratio (SNR) can be obtained and aliasing avoided. The current lowpass filter in use is a presummer that sums up N adjacent values per output. With filters specifically designed to surpress noise in certain frequency bands, a more adequate performance can be obtained.

This thesis describes the design and performance evaluation of an anti-alias pre-filter for the nadir looking coherent airborne radar POLARIS. Masking clutter from the surface of the ice sheet is unwanted and is characterized as noise. Also thermal noise must be handled, which at a point is much greater than the masking surface clutter noise. Clutter from the surface of the ice is a big issue, when employing an ice sounder. A signal return from the subsurface, will at the same time instant result in a recieved signal from the surface. Several external parameters such as the altitude of the radar, the ice surface characteristics and the signal attenuation in the ice are of crucial importance, when investigating the recieved power in the radar system. POLARIS is a low altitude airborne ice sounder, and the analysis is carried out with a flying height of 600 meters. For airborne radars flying at a relatively low altitude, the angles for which the clutter arises, will increase more rapidly for smaller penetration depths in the ice.

POLARIS relies on accurately measuring the time delay between the transmitted pulse and the returned radar signal. The anti aliasing filter must consequently have linear phase. The requirement can easily be met by a symmetric filter impulse response,

[1]Polaris is an abbreviation for: Polarmetric Airborne Radar Ice Sounder

[2]Nyquist theorem for complex signals states that the PRF must be greater than the signal bandwidth

which is presented in section 2.2. Hardware limitations in the onboard proccessing is the limiting factor, and a proper implementation architecture must be defined.

The proposed designs are based on filter design in Matlab, this involves weightning of filter frequency bands, that leads to an efficient noise suppression. For the scope of this project several simplifications and assumptions are made with respective to the study and implementation of models for the applied radar theory.

CHAPTER 2

Theory

2.1 Radar geometry

Airborne ground penetrating radars are used to map the subsurface of the earth. Figure 2.1 [3] gives an overview of the geometry associated with imaging radars. The radar is equipped with a SAR[1] configuration. A synthetic aperture is used, because of the practical infeasibility of flying with a big physical aperture to obtain a good resolution. As seen from figure 2.1 the antenna is looking to its right, and the radar beam illuminates an area, with a swath width w_g, known as the antenna footprint. The antenna is dimensioned with the physical lengths W and l. The platform moves in the along track direction also known as the azimuth direction, while the nadir track refers to the track directly beneath the platform. The ground range is the perpendicular distance from the nadir track to a given target. The slant range is the distance directly from the radar to the target introducing a incident angle θ from nadir. The slant range will be refered to as R or "the range to the target".

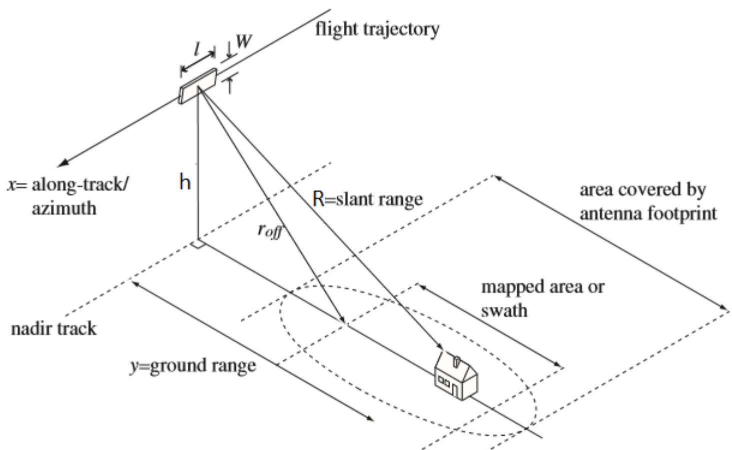

Figure 2.1: Geometry associated with a radar looking to its side.

[1] Abbreviation for Synthetic Aperture Radar

The coverage of the antenna depends on the distance R_{off} and the angular beamwidth, that can be approximated to $\beta_a = \frac{\lambda}{l}$ [3] where λ is the wavelength. Consequently the scattering contributions will often be confined within big volumes, which leads to a poor resolution. However the resolution is improved by applying a signal proccessing technique known as pulse compression[2]. After pulse compression the resolution in slant range can be improved to [3]

$$\rho_r = \frac{c}{2B} \tag{2.1}$$

Where B is the pulse bandwidth. POLARIS is a nadir looking ice sounding radar with the same geoemtry as a SAR. However a key difference exists. The nadir looking radar looks down into the subsurface of the ice, while a "SAR" in general is used to map the features on the ground. This implies a significant attenuation of the subsurface nadir signal for the nadir looking radar, which in general is not the case when referring to a SAR.

The range R can be expressed in term of the incident angle. Applying simple geometry reveals that the range can be expressed in terms of incident angle θ and the height above surface h

$$R = \frac{h}{cos(\theta)} \tag{2.2}$$

With the range R expressed as a function of the incident angle, the recieved power in the radar system can also be expressed as a function of incident angle, which is presented in section 2.3. Before introducing the recieved power in a radar system, other important aspects must be introduced. This involves a characterization of the noise that must be suppressed, and furthermore the resolution of the nadir looking radar, along with the area illuminated by the transmitted pulse.

2.2 Noise

Surface clutter is of great concern in radar systems and specially when related to ice sounding. The clutter signals are unwanted signals that arises from the surface of the ice, due to the curvature of the pulse waveform. Figure 2.2 [10] illustrates the clutter returns from the surface corresponding to the nadir signal, when it has travelled to a depth z. The nadir-looking radar can be seen as flying in the along track direction, defined as x in the coordinate system. The clutter return as seen both on the left and the right, is an example of the location of the clutter origin, associated with the specific nadir signal at depth z. The relation between the incident angle of the surface clutter and the depth z, is mathemathically described in equation 2.12.

[2]With pulse compression the range and azimuth resolution is improved, by modulating the transmitted signal and correlating the return with the transmitted pulse (matched filtering)

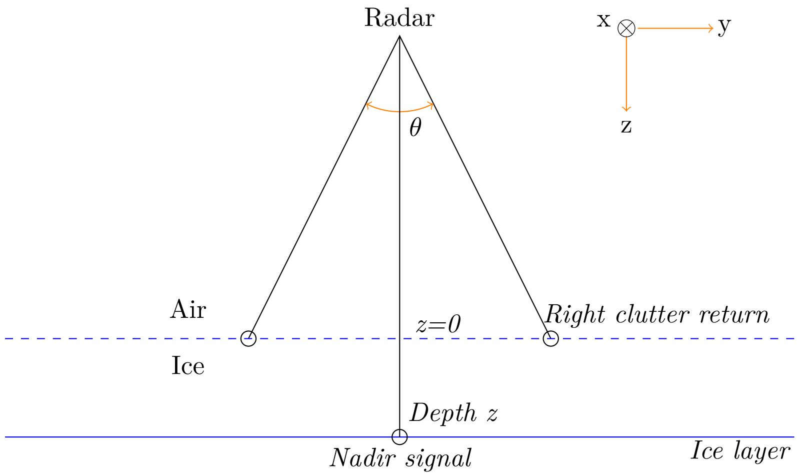

Figure 2.2: Nadir sounding; surface clutter.

As the depth z increases the incident angle θ also increases. The radar is located at a height h, which also determines the direction of arrival of the surface clutter (DOA), which can be visualized from the figure. The power recieved from the clutter returns is only significant up until the maximum doppler frequency, and thermal noise is then of greater concern. The thermal noise from the antenna is given by [5]

$$P_n = KT_aB_n$$

Where K is Boltzmann's constant, T_a is effective antenna temperature in Kelvin and B_n is the noise bandwidth. The effective antenna temperature can be calculated from [7]

$$T_a = T_i(\Gamma - 1) + T_g\Gamma$$

T_i is the is the brightness temperature of the ice and T_g is the brightness temperature of the sky. Γ is the surface reflectivity of the air ice interface illustrated as the dashed line in figure 2.2. Because of normal incidence the surface reflectivity reduces to R_{01}^2, which is the the same quantity introduced in equation 2.10. The galatic noise is set to a temperature of 200 Kelvin [9]. Noise in the antenna is not the only source to thermal noise, and the noise power in the reciever must also be included. When the reciever noise is included the total thermal noise power becomes

$$P_n = KT_0(F_n - 1)B_n + KT_aB_n \tag{2.3}$$

Where the reference temperature is $T_0 = 290K$ and B_n is the reciever noise figure.

2.3 Illuminated surface area

By doppler processing[3] the clutter from the along track direction is effectively suppressed. What remains is the clutter from the across-track direction. The blue areas as seen from figure 2.3 [7] is the pulse limitted footprints, where as the red areas are doppler processed footprints at different times $t_1 ... t_4$.

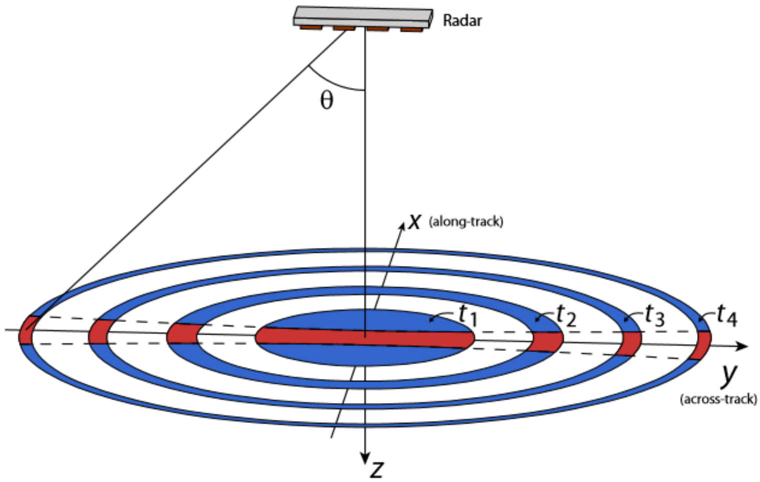

Figure 2.3: Footprint.

The azimuthal bandwidth of the SAR is a given value and it is provided by the supervisor. The bandwidth is given by

$$B_{az} = 35\ Hz$$

The total doppler shift across the synthetic aperture is two times the doppler frequency, which equals the azimuthal bandwidth. The doppler frequency is given by two times the velocity of the radar divided by the wavelength $f_d = \frac{2v}{\lambda}$. The factor 2 accounts for the two way doppler shift. When a target is located far behind the radar in the along track, the radar to target velocity is approximated to be -v. As the radar approaches the target the velocity becomes 0 and again increases to v, as the radar passes the target and the target is far behind the radar. This gives rise to a linear doppler variation near the target, and a linear frequency modulated signal [3]. The resolution of a linear frequency modulated signal is

$$\rho_t = \frac{1}{B_{az}}$$

[3] Matched filtering process in azimuth to obtain high resolution

Where the bandwidth B_{az} depends on the matched filtering in the postprocessing of the data. The azimuth resolution is then obtained by multiplying with the velocity of the radar v.

$$\rho_x = \rho_t v = W_x$$

The azimuth resolution is essentially the distance in azimuth two targets must be seperated, for the radar to differentiate between the two targets. The azimuth resolution is here denoted as W_x, which describes the along track dimension of the doppler processed footprint. The along track width is assumed to be constant. The area of the footprints at different time instanses after doppler processing is then obtained by calculating the corresponding across-track width W_Y. The across-track width can be calculated as [8]

$$W_y = \sqrt{R^2 - h^2} - \sqrt{r^2 - h^2}, \qquad r \geq h \tag{2.4}$$

Where R and r is the radius of the wavefront and waveback of the transmitted pulse as seen from the radar. Therefore the radii can completely be described by the altitude of the radar, the depth z at which the pulse has propegated to and the resolution in slant defined in equation 2.1. However for a pulse limited footprint the across-track width corresponds to the length in the first cell, and it is in that case calculated from

$$W_y = 2\sqrt{R^2 - h^2}, \qquad r \leq h \leq R \tag{2.5}$$

2.4 Recieved power in the radar system

With the geometry associated with radar systems is defined, it is desirable to investigate the parameters that characterize the power recieved in a radar system.

This purpose of this section is to express the power recieved in a radar system as a function of the incident angle, for straightforward analysis. This involves the backscattering at nadir for internal layers, which is a specular reflection. The general form of the radar equation for recieved power as seen from equation 2.6, will be used to calculate the recieved power from internal reflections in the ice, and furthermore it will be used to calculate the recieved power from surface clutter returns. The derivation is based on a number of key equations. This involves pages [11-15] in Ice sounder note written by Ulrik Nielsen. [7]

The recieved power in the radar system is described by the radar equation

$$P_r = \frac{P_t G_t G_r \lambda^2 \sigma}{(4\pi)^3 R^4 L} \tag{2.6}$$

In table 2.1 the different parameters are listed

Table 2.1: Radar equation parameters.

Parameter	Unit of measure
P_r: Recieved power	[W]
P_t: Transmitted power	[W]
G_t: Transmit antenna gain	[dB]
G_r: Recieve antenna gain	[dB]
λ: Wavelength	[m]
σ: Radar cross section	$[m^2]$
R: Range to target	[m]
L: Loss factor	[dB]

The loss factor for the propagation in ice is given by

$$L = 10^{0.1 \int_0^z a(z')dz'} \tag{2.7}$$

Where $\alpha(z)$ is the two-way attenuation coefficient at depth z in dB. For simplicity the attenuation coefficient is assumed constant, and hereby independent of depth. (2.3) reduces to

$$L = 10^{0.1a \int_0^z dz'} \leftrightarrow L = 10^{0.1az} \tag{2.8}$$

In order to calculate the recieved power the radar cross-section must be modelled. The cross-section contains the reflection characteristics of the target in interest. The scattering from the internal layers of the ice is in this section modelled as a specular reflection. The radar cross section for a specular reflection is

$$\sigma_{ss} = \pi T_{ss} R^2 \tag{2.9}$$

Where T_{ss} is the Fresnel reflectivity, R_{12} and R_{01} are respectively reflections coefficients for the reflection at internal layers and from reflections of the surface. The Fresnel reflectivity is then given by

$$T_{ss} = R_{12}^2 (1 - R_{01}^2)^2 \tag{2.10}$$

When inserting the known reflection coefficents, the radar cross-section becomes

$$\sigma_{ss} = \pi \left(\frac{9.25 \cdot 10^{-4}}{\epsilon_{ice}} \right)^2 \left(1 - \left| \frac{1 - \sqrt{\epsilon_{ice}}}{1 + \sqrt{\epsilon_{ice}}} \right|^2 \right)^2 R^2 \tag{2.11}$$

The depth z at which the signal has propagated through the ice, can be expressed in terms for the incident angle θ, the height h and the relative permativity of ice.

$$z(\theta) = \frac{h\,(1 - cos(\theta))}{\sqrt{\epsilon_{ice}} cos(\theta)} \tag{2.12}$$

The radar cross section can now be further specified by evaluating (2.7) with the known values. The relative permativity of ice is assumed to be $\epsilon_{ice} = 3.15$, and the radar cross sections becomes.

$$\sigma_{ss} = \pi 2.5 \cdot 10^{-7} R^2 \tag{2.13}$$

From (2.2) in the previous section an expression for the range R was shown. The radar equation can now be expressed as a function of incident angle θ. The cross-section (2.10), the penetration depth (2.9) and the expression for R (2.2) is inserted into the radar equation (2.3). And the recieved power is given by

$$P_r(\theta) = \frac{P_t G_t G_r \lambda^2 \pi \cdot 2.5 \cdot 10^{-7} cos(\theta)^2}{(4\pi)^3 h^2 10^{0.1az}} \tag{2.14}$$

The expression for the recieved power as a function of incident angle θ is later used to determine the recieved power from the clutter returns, and the reflected signal from nadir. However the propegation in the air is assumed lossless and thus no loss is included in the radar equation, when analysing the clutter returns. When the signal travels through the air and hits the surface of the ice, the signal will be refracted, as described by Snell's law[4]. This gives rise to a refraction gain that can be accounted for in the radar equation by including it as a gain factor. This gain factor factor will not influence the recieved power significantly, and therefore it is neglected in this project.

It is in generel a difficult task to model the radar cross section for ground penetrating radars. When modelling the radar cross-section for the surface of the ice, it can theoretically be modelled by the Inchoerent Kirchoff Model (IKM) or the Small Pertubation Model (SPM) [7]. In these models the surfaces are assumed to be normally distributed with a standard deviation σ_h, and a correlation length λ_h. These statistical parameters can be hard to determine because of the uncertainty of the surface roughness in a specific situation. In the implementation, these radar cross-sections for surface returns are instead based on measurements of the normalized backscatter coefficients, denoted as *sigma naught*

$$\sigma^0 = \frac{\sigma}{A} \tag{2.15}$$

Where A is the illuminated surface area. The radar cross-section is based on few measurements, and will be extrapolated in order to calculate the decreasement of the backscatter coefficient as the depth z increases. However when investigating the scattering of the internal layers of the ice, where only the scattering from nadir is calculated, the radar theoretical cross-section σ_{ss}, presented in equation 2.13, is used.

[4]Snell's law describes the relationship between incident angle and angle of refraction for a signal passing through two different media

2.5 The Finite Impulse Response filter

As previously mentioned the phase between the transmitted and returned signal must be linearly related. Therefore the phase response of the filter must also be linear. When this condition is met, the delay introduced through the filter is the same for every frequency. Linear phase is easily achieved with a finite impulse response filter. A FIR filter with length M, output y(n) and input x(n) is described by the difference equation [2]

$$y(n) = b_0x(n) + b_1x(n-1) + ... + b_{m-1}x(n-M+1) = \sum_{k=0}^{M-1} b_kx(n-k) \tag{2.16}$$

Where b_k is the filter coefficient for delayed input also known as the feed-forward elements. As seen the FIR system does not have delayed outputs, this classifies it as a finite impulse response filter (There is no feedback). The impulse response of the filter is defined by the resulting output when a kronecker delta function $\delta(n)$ is applied to the input. The linear phase condition for the FIR filter is then met when its impulse response satisfies [2]

$$h(n) = \pm h(M-1-n), n = 0, 1, ..., M-1 \tag{2.17}$$

Which means that the filter coefficients must be either symmetrical or anti symmetrical around the middle coefficient, to obtain the desired linear phase. The proposed design, presented in the implementation, is based on the Firpm[5] design in Matlab. The frequency response of such filters shows an equiripple behaviour, and are called equiripple filters.

The windowing and frequency sampling methods are commonly used for designing linear phase FIR filters. However using these design methods, it is hard to accurately obtain the desired pass - and stopband frequencies. The equiripple design is seen as a optimum design, where the error between the desired and realizable frequency response is uniformly spread across the pass - and stopband.

[5] The design is based on Parks-McClellan optimal FIR filter design in Matlab

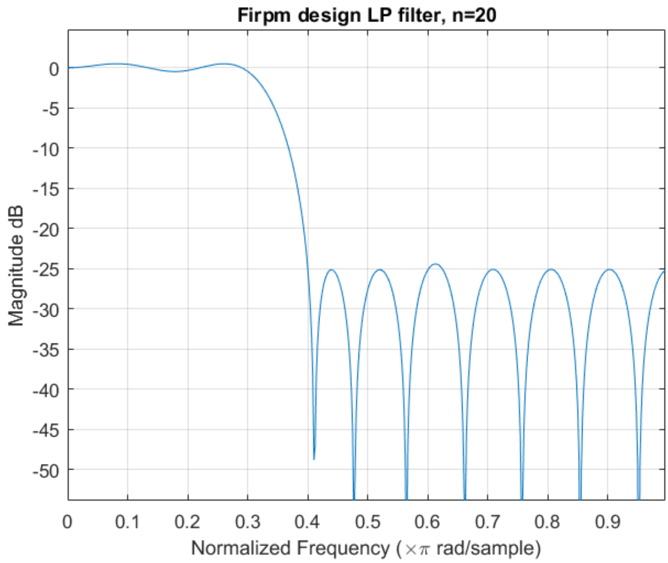

Figure 2.4: Equiripple magnitude response.

Figure 2.4 [10] shows the frequency response af a linear phase FIR filter, created with Parks-McClellan optimal algorithm. As seen ripples are present in both passband and stopband. However an oppertunity exists to minimize the passband ripple and stopband attenuation, whilst using optimal design methods. It is possible to define transition regions, these regions are also called don't care bands. In these bands the error is not minimized and they therefore have much less attenuation. This gives a better optimization in the bands of interest, and the design method becomes rather attractive in relevant applications [1].

2.6 Sampling and decimation

Sampling a time domain signal leads to periodicty in the frequency domain. The spectrum $X(f)$ of a discrete time signal $x[n]$, that is obtained by sampling the time domain signal is given by [4]

$$X(f) = \sum_{n=-\infty}^{\infty} x[n] e^{-j2\pi f n}$$

From the discrete Fourier transform it is seen that the multiplication with the complex sinusoid is what introduces the periodicity in the spectral domain. Replicas will therefore be introduced at integer multiples of the sampling frequency. The sampling frequency of the along track signal equals the pulse repetion frequency. This means that the recieved signal is sampled with a sampling frequency fs=2500. Since a high SNR ratio is desired the signal is low pass filtered and decimated by a factor 40. Figure 2.5 [10] gives an overview of this process, but thats not excatly how it is implemented.

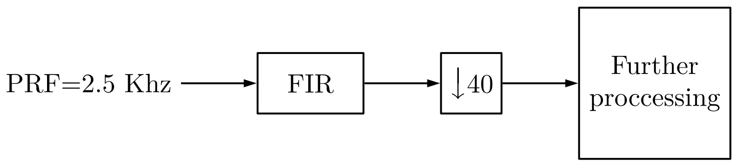

Figure 2.5: Inefficient decimation.

By decimating with a factor M the complex signal must be limmited by

$$\frac{-f_s}{2M} : \frac{f_s}{2M}$$

Using the decimation factor $M = 40$ gives the total bandwidth

$$BW = \frac{fs}{M} = \frac{2500}{40} = 62.5Hz$$

Decimation will in the frequency domain lead to spectral aliasing. Since the replicas located at integer multiples of the old sampling rate, will move down to integer multiples of the new sampling rate.

The process of filtering and then downsampling is known as decimation, and is commenly implemented in this way. However it is inefficient since calculated samples are discarded. This process more accurately happens in the FIR filter. The decimation is therefore not the process of discarding M values from the output of the low pass filter, but instead the process of not calculating the outputs which will not be used. This is determined by the decimation factor M. As the output is a function of the past inputs only, the filter does not have any feedback, as presented in the previous section. Therefore only the outputs which will be used is calculated. This is done by dividing the filter in to several subfilters corresponding to the number of available channels. The number of channels is 4. [7]. The process is described in figure 2.6. [10]

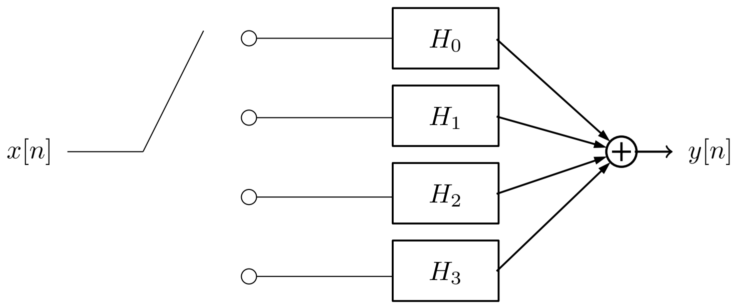

Figure 2.6: Efficient polyphase decimation.

Before the sampled input signal $x[n]$ enters the polyphase filter, the switch chooses every 40th sample, defined by the decimation factor $M = 40$, and the rest of the samples are discarded. The 4 subfilters are then summmed to reproduce the output signal $y[n]$. Each time a set of values has been filtered through a channel, the channel is flushed to make room for the new decimation. Therefore figure 2.6 does not completely represent the process, and it is rather ment as a primitive overview. The polyphase decimation sets a limit for the maximum length of the filter. Decimating with a factor 40 with 4 channels defines the hardware limitation, and the maximum length of the FIR filter is then the product of number of channels and decimation factor.

$$N_{FIR,max} = 40 \cdot 4 = 160$$

However the maximal filter length does not fulfill the symmetry condition for achieving linear phase. Therefore the filter length is reduced to 159, and linear phase can then be achieved.

2.7 Integrate and dump filter

Considering a simple decimation filter, with a decimation factor that equals the filter length, it is desired to assess the the signal to noise improvement of the filtering process. Without any prior knownledge about the signal and noise levels, it is not possible to calculate absolute signal-to-noise ratios, however the SNR improvement is of interest. The SNR improvement can be defined as

$$SNR_{IMP} = \frac{S_{tot}/N_{Bfilt}}{S_{tot}/N_{tot}}$$

Where the numerator is the ratio of the total signal power before filtering and decimation and the total noise power within the signal bandwidth after filtering and decimation. The denominator is the ratio of the total signal power before filtering and decimation and the total noise power before filtering and decimation.

The filter is defined by constructing a impulse response consisting of 40 ”ones” and it is zero elsewhere. The analysis signal is a square wave in frequency with a bandwidth of 35 Hz, and additive noise. In figure 2.7 the frequency respose of the filter is shown on a linear scale. From basic frequency domain analysis it is well known that a rectangular pulse has a $\frac{sinc(x)}{x}$ like spectrum. The Fast Fourier Transform (FFT) is used to obtain the frequency response. Initially a function that implements the discrete Fourier transform was written. With a need for high resolution, the number of discrete Fourier transform points was too great for the function, with respect to the calculation time. Instead MATLAB's FFT function is used to calculate the discrete Fourier transform. The function uses a efficient FFT algorithm, and the number of FFT points is specificed in the function. The signal to be filtered is a square wave in frequency with additive noise of amplitude 0.1, as shown in figure 2.7.

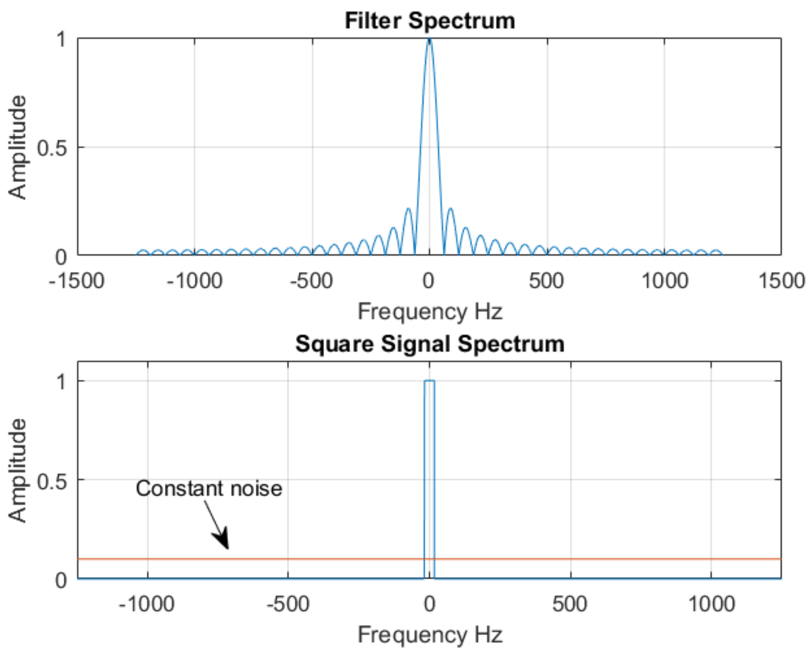

Figure 2.7: Sinc spectrum, and square spectrum with additive noise.

Filtering the square signal spectrum with the sinc filter results in the filtered signal in figure 2.8. Due to the sampling that leads to periodicty in the frequency domain, the spectral replicas gets centered around multiples of the sampling frequency. By decimating with a factor 40 in time will move the sample rate down by a factor 40 $\frac{fs}{40}$. In frequency this corresponds to spectral folding, and the original stop bands will fold into the passband, effectively adding the stopband noise to the passband noise.

The decimation is carried out by evaluating the power in the each frequency stopband after filtration. With a signal bandwidth of 35 Hz, a sampling frequency of 2500 Hz and a decimation factor D=40, the stopbands are located in multiples of 62.5 Hz

$$\frac{fs}{D} = \frac{2500\ Hz}{40} = 62.5\ Hz$$

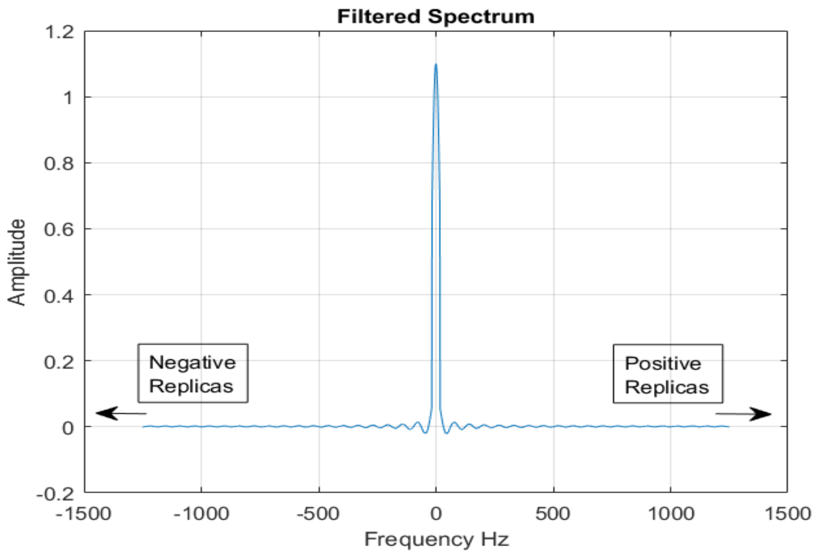

Figure 2.8: Filtered square pulse.

After filtration and decimation the SNR improvement of the filtering process is calculated to be

$$SNR_{IMP} = \frac{S_{tot}/N_{Bfilt}}{S_{tot}/N_{tot}} = 8.5\ dB$$

CHAPTER 3
Implementation

In this chapter the various implementation stages will be gone through, and the written MATLAB programs is mainly presented from a mathematical point of view, and by including plots for visualization. The first section presents the firpm design method in Matlab, and the radar equation is then implemented with the use of the presented theory and emprical measurements. After the implementation the recieved signal and noise power is examined, and several cases are shed light on. These cases involves recieved power for smooth and rough ice surfaces, and they also involves a comparison of the signal attenuation for cold and warm ice.

3.1 FIRPM design

The design is based on the inbuilt function *firpm* [11] in MATLAB. The design method follows the syntax:

$$b = firpm(n, f, a, w)$$

Where the the input variables are the order, a frequency vector, and an amplitude vector. w is a vector containing weights for each frequency band, used for the optimization. It is an optional variable, and with no specification it is by default set to unity. In this first implementation stage the band weightning will not be specified. The output b is the calculated filter coefficients.

f contains the normalized frequency band edges, which are normalized by the nyquist frequency. The first frequency band is the pass band, which lie in the interval [0:17.5] Hz. The rest of the frequency bands are placed at integer multiples of the new sampling frequency (decimated) 62.5 Hz each having a bandwidth of 35 Hz.

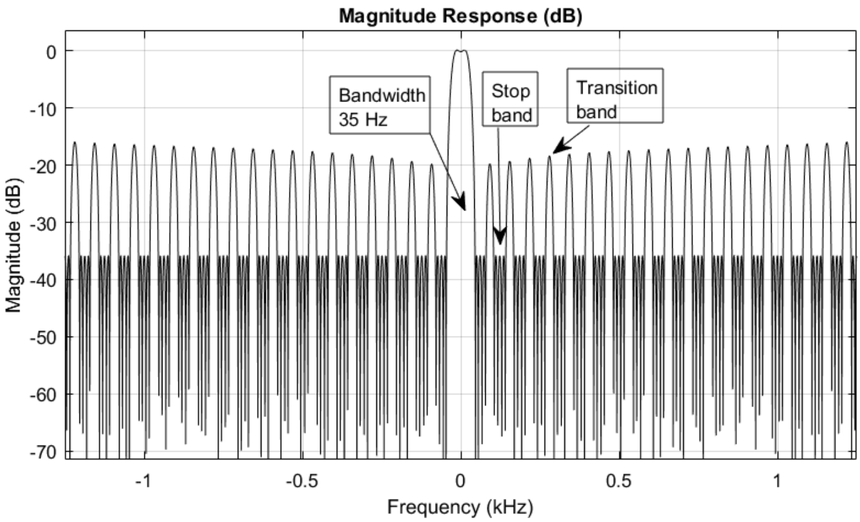

Figure 3.1: FIRPM magnitude response without weights.

In this specific example the filter length is N=160. This length is later reduced to achieve linear phase.

3.2 Relating the radar equation

In order to suppress the thermal noise and surface clutter recieved in the radar system, the recieved power hereof has to be calculated. This is done with the theroy presented in section 2.2 and 2.3. This section presents the implementation of the radar equation, with use of empirical data of backscatter diagrams from smooth and rough faces, and by the use of provided antenna radiation patterns.

As the first step, the parameters in the radar equation must be related. The radar equation 2.6 is written here again for the sake of overview.

$$P_r = \frac{P_t G_t G_r \lambda^2 \sigma}{(4\pi)^3 R^4 L}$$

A fixed number of points $nsamp = 90000$ is chosen to represent the parameters in the radar equation excluding the transmitted power P_t (peak power) and the wavelength λ, that are both constants. The number of points or samples can be arbitrarely chosen, but it is chosen to match the number of samples used in the several tests presented in chapter 4. In table 3.1 an overview of the radar equation parameters is given. All parameters are expressed as a function of incident angle θ.

Table 3.1: Radar equation as a function of θ.

Parameter	Clutter	Signal	Remark	Unit
Incident angle	$\theta_c = (0 : N : 89)$	-||-	$N = \frac{\theta_{max} - \theta_{min}}{nsamp - 1}$	Degree
Depth	$z_c(\theta) = \frac{h(1-cos(\theta))}{\sqrt{\epsilon_{ice}} cos(\theta)}$	-||-		m
Range	$R_c(\theta) = \frac{h}{cos(\theta)}$	$R_s = z + h$	Clutter on surface and depth z	m
Loss factor		$L = 10^{0.1az}$	Loss factor lossy ice propagation	$\alpha = dB/m$
Gain	$G(\theta)$	G_{nadir}	Signal gain, max gain	dB
Backscatter Coefficient	$\sigma_c \theta = \sigma_c^0 A(\theta)$	σ_s	Empirical meas. & Theoretical model	dB

As seen no loss is accounted for in the clutter signal. It is hereby assumed that the attenuation of the clutter signal, whilst it propagates in the air, is insignificant. As mentioned, every parameter is a vector containing 90000 samples. This comes from the defintion of the incident angle seen in the second column of table 3.1. The used notation is not strictly mathematical, but is instead the notation used in MATLAB. The vector containing θ should be understood as a vector having the values ranging from 0 to 89, equally spaced with the stepsize N as it appears from the remark. An important parameter that is not included in the table is the doppler frequency vector presented in section 2.1.1. To evaluate the maximum doppler frequency, the wavelength and the speed of flight must be defined along with other "external" parameters. Table 3.2 summarizes the used external parameters

Table 3.2: External radar parameters.

Parameter	Numerical value
Height above surface	$h = 600\ m$
Flight speed	$70\ m/s$
Radar operating frequency	$f_{op} = 435\ MHz$
Wavelength	$\lambda = \frac{c}{f_{op}} = 0.6892\ m$
Ice relative permittivity	$\epsilon_{ice} = 3.15$

And the maximum doppler frequency becomes

$$f_d = \frac{2v}{\lambda} sin(\theta_{max,rad}) = 203.1096Hz$$

The maximum doppler frequency sets the boundary for the surface clutter power recieved in the radar system, and the analysis is carried out with the doppler frequency ranging from 0 to 203 Hz. At higher frequencies the thermal noise dominates over the surface clutter, which is presented in section 3.4. The direction of arrival of the clutter (DOA) arises from angles ranging from 0 to approximately 90 degrees. When the incident angle approaches 90 degrees it corresponds to very large depths in the ice, and there is practically no signal left. The DOA is also greatly dependent on the altitude of the radar. The relationship is seen in figure 3.2.

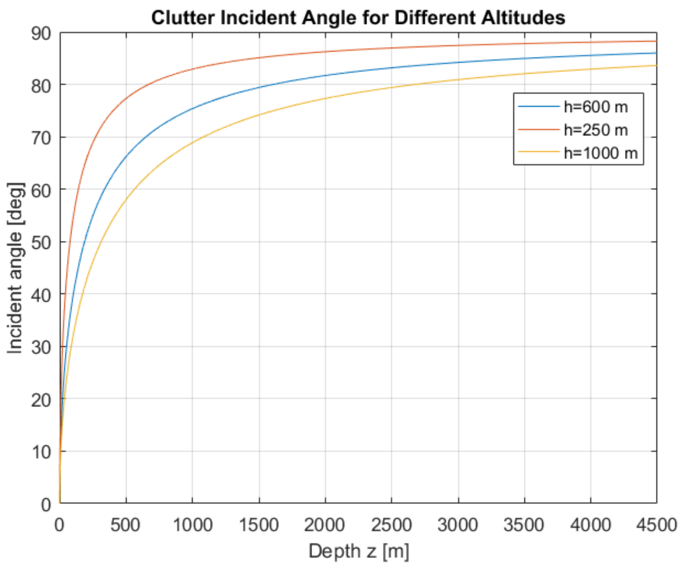

Figure 3.2: Clutter DOA for heights 250m, 600m, 1000m.

The blue curve illustrates the actual scenario for which the FIR filter must be designed. That is a height of 600 meters. At lower altitudes the clutter incident angles increases rapidly, and at higher altitudes the increase happens at a slower rate. As seen from table 3.1 The gain is also a function of θ. In figure 3.3 a plot of the along and cross track antenna diagrams is seen [9]. The along-track gain smoothly decreases until a angle of around 150 degrees, while the across-track antenna diagram has several side lobes. The nulls in the cross-track diagram means that, the antenna itself will suppress clutter corresponding to those angles. The plottet antenna diagrams each consists of 361 samples, and they are therefore interpolated to match the number of used samples in the program.

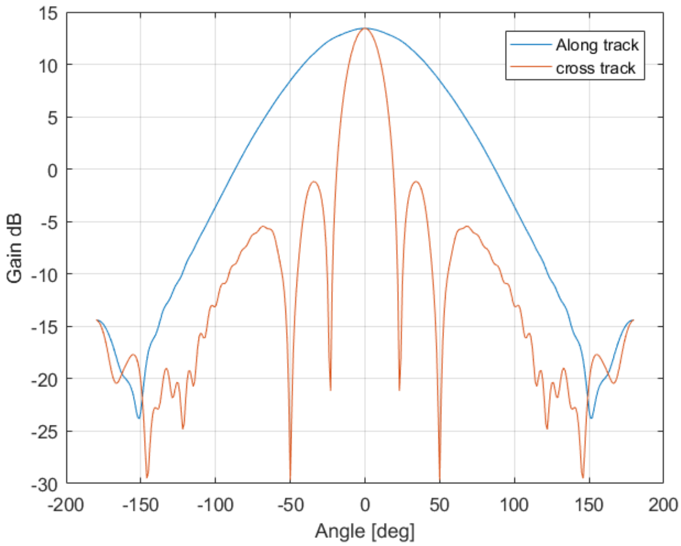

Figure 3.3: Along and cross track antenna diagram.

3.3 Backscatter

The radar cross sections used are based on empirical values provided by the supervisor [9]. The provided data is the normalized radar cross sections, and they must therefore be multiplied with the area of a resolution cell.

Smooth surface [Deg]	Smooth surface [dB]	Rough surface [Deg]	Rough Surface [dB]
0	0	0	0
0.3	-15	1	-2
4.3	-60	6	-10

Table 3.3: Backscatter data for the rough and smooth surface.

Beyond the known values it is principle unkown what happends afterwards. Therefore the backscatter values must be extrapolated, and afterwards interpolated to match the number of samples used in the program. Also the backscatter coefficient at 0° for the surface and bottom of the ice must be taken into account. Table 3.3 gives an overview of the nadir backscattering coefficients.

$\sigma_{nadir,ss}$	15 dB
$\sigma_{nadir,sb}$	0 dB
$\sigma_{nadir,rs}$	0 dB
$\sigma_{nadir,rb}$	-20 dB

Table 3.4: Nadir backscatter: Smooth and rough ice surface and bottom.

Since only the first strong return from the bottom of the ice at 0° is of interest, it is not necessary to include a scattering pattern for the bottom of the ice. However the scattering pattern for the surface of the ice must be extrapolated. In figure 3.4 the extrapolation of the backscatter values for the rough and the smooth surface is plotted.

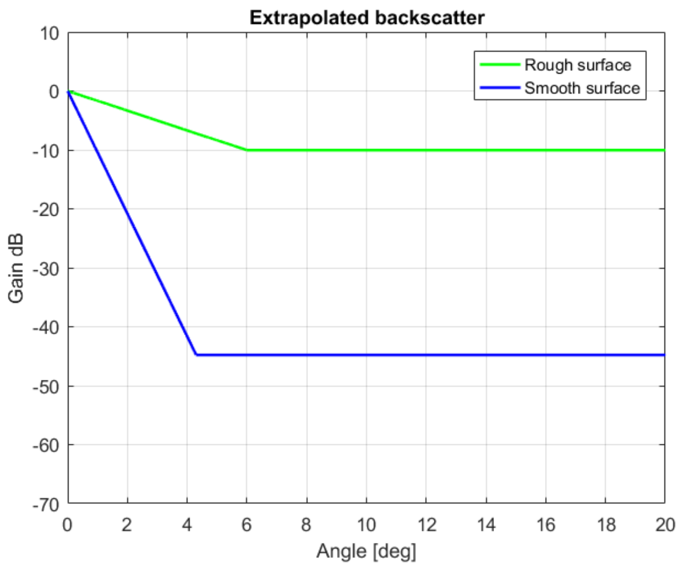

Figure 3.4: Extrapolated backscatter diagram for the rough and smooth surface.

The backscatter coefficients can be extrapolated under several assumptions. Here it is assumed that the backscatter for the rough surface is constant after the last measured value at 6 degrees. This corresponds to a constant gain of -10 dB at 6 degrees and hereafter. The same assumption is made for the smooth surface, which should be constant after 4.3 degrees. When including the nadir backscatter coefficient $\sigma_{nadir,ss}$=15 dB, it corresponds to a constant gain of -45 dB after 4.3 degrees. When modelling the internal layers of the ice, the radar cross section for a specular reflection presented in section 2.4 is used. After implementation of equation 2.9 the backscatter coefficient is roughly -71 dB. And for the bottom of the ice, the values in table 3.3 apply. In the case for a rough bottom the nadir backscatter coefficient is $\sigma_{nadir,rb} = -20\ dB$. Furthermore the attenuation in the ice is a significant factor when determining the recieved power in the radar system. Two values for the attenuation in the ice is used. For cold ice the attenuation in the ice is 2 dB/100m at for warm ice the signal is attenuated with 10 dB/100m [9].

3.4 Recieved signal and noise power

With the radar equation implemented in MATLAB, the recieved power from the nadir signal, and the noise power (thermal and clutter) can be visualized in order to understand, to which extent the noise must be supressed in the filter. It should be noted that the implementation of the thermal noise deviates from the theory presented. This is due to the fact that the radar equation should take the pulse compression gain into account, which is further elabroated in this section. This is equivalent to dividing the thermal noise with the time-bandwidth product of the modulated pulse, which equals the pulse compression gain (PCR)

$$PCR = B\tau$$

Where the bandwidth is 85 MHz and the pulse length can be set to $\tau = 2\mu\ s$, which is a typical pulse length used in POLARIS [9]. Without taking the pulse compression gain into account the thermal noise is the constant value of

$$P_{therm} \approx -122\ dBW$$

Which is also seen in figure 3.5. By dividing the thermal noise with the time-bandwidth produce, and thereby accounting for the pulse compression gain, the new thermal noise level becomes

$$P_{therm} = -144\ dBW$$

In the following implementation the thermal noise is neglected, and the filters are designed specifically to suppress only the clutter arising from the surface of the ice.

3.4.1 Recieved power for the rough surface

In figure 3.5 [10]. The three recieved components are illustrated. The clutter power, the constant thermal noise power and the signal power.

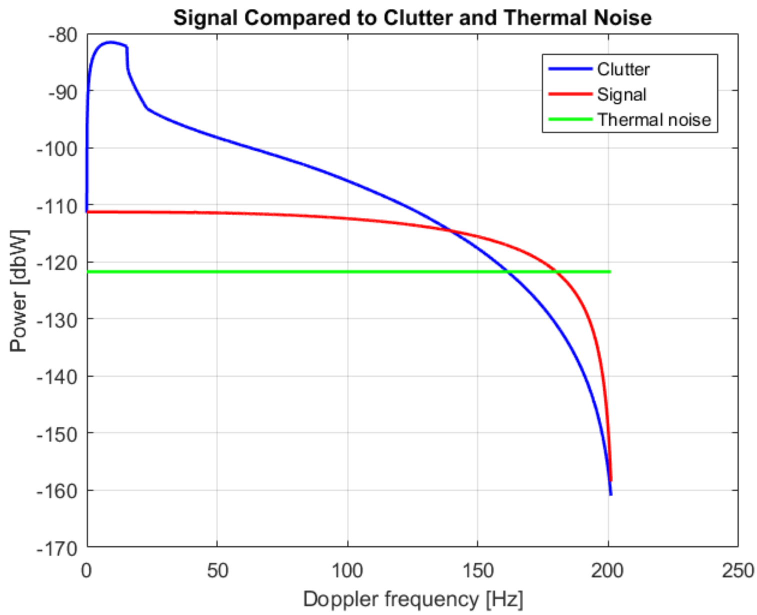

Figure 3.5: Rough surface: Power recieved until max. doppler for cold ice.

The signal power does not depend on the doppler frequency, and should more correctly be plotted against the depth z. However the depth z corresponds to a certain doppler frequency. The noise is limitted by the maximum doppler frequency, which for the signal in this case corresponds to a depth in the ice of 2000 meters. The surface scattering is for a rough surface, and for the signal the attenuation in the ice is $\alpha = 2dB/100m$ (cold ice) [9]. The thermal noise is constant in every frequency band, and the effective noise to be suppressed in the filter is then the contribution from the constant thermal noise and the clutter returns. In the following the filter is designed to only effectively suppress the surface clutter returns.

As described the stopband frequencies are located at multiples of the 62 Hz, with a bandwidth of 35 Hz. The first three stopband frequency ranges are seen in table 3.5. Which is the frequency bands of interest in the following implementation.

Table 3.5: First three stopband frequency ranges.

Stopband	Frequency [Hz]
1	$[45 : 80]$
2	$[107.5 : 142.5]$
3	$[170 : 205]$

The FIRPM design with unity weighting already suppresses approximately -35 dB, which is seen from figure 3.1. Therefore there should be no need to apply specific weights in these bands. By filtering and decimating the recieved clutter, with unity gain in the bands of interest it is in figure 3.6 seen that the clutter is effectively supressed. The envelope of the green curve can be considered as the filtered clutter. The changing form is caused by the frequency domain filtration.

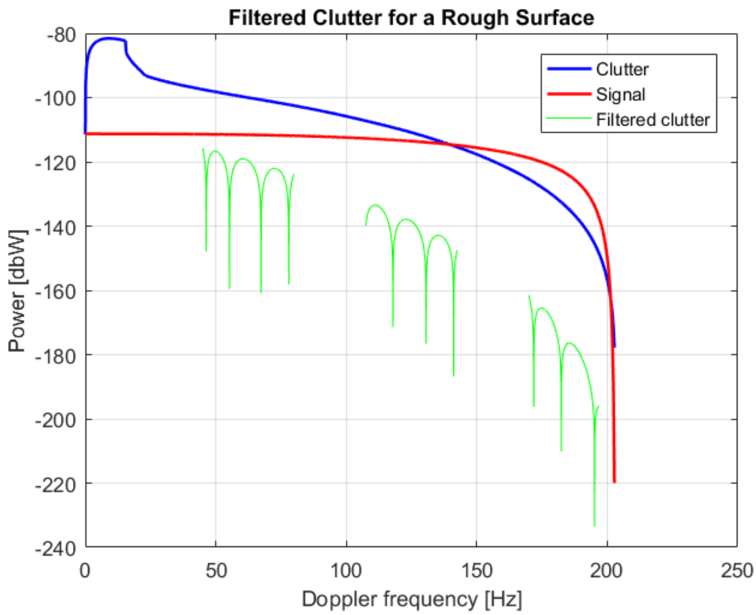

Figure 3.6: Rough surface: Filtered clutter.

Even though no weighting factors are used, it can be necessary to include them when considering the overall performance of the specific design case. To properly investigate the deeper layers of the ice and the bedrock, the following implementation is carried out by comparing the recieved clutter and signal power to a depth z the nadir signal has travelled. In figure 3.7 the power recieved is plotted against the depth z. The blue curve illustrates the recieved clutter. From the plot the following four important interpretations are made

- The surface clutter is masking the signal for near surface layers
- The SNR is positive in region of approximately 200 to 1700 meters
- The SNR is negative for deeper layers $>$ 1700 meters
- The bedrock exhibits a powerful return

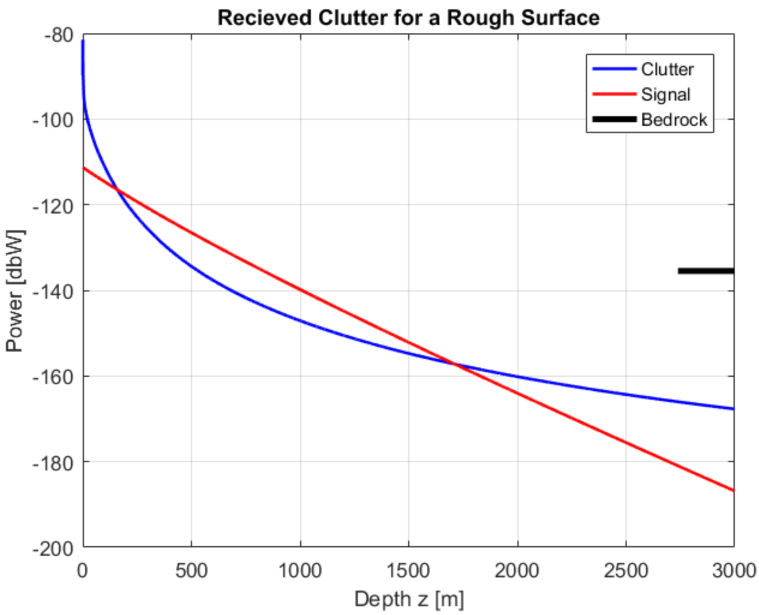

Figure 3.7: Rough surface: Clutter and bed return for cold ice.

The black bar illustrates the powerful return from bedrock. The bedrock is set to start at 3000 meters, and the bar is therefore not representative of where the bed begins, but it is rather included to visualize the recieved power (-135 dbW). For the It is seen that the the clutter level is lower than the return from bedrock, however a high SNR is still desired and filter weightning is necessary. For a complete implementation of the radar equation the pulse compression gain must be taken into account.
To simulate the bedrock return, the backscatter coefficient at 0° for a rough ice bottom is used

$$\sigma_{0,nadir} = -20\ dB$$

[9]

Another interesting scenario is when the attenuation is much higher. For warm ice $\alpha = 10\ dB/100m$, which is 5 times more than for the cold ice. By changing the signal attenuation to the attenuation of warm ice, it can clearly be seen from figure 3.8 that the signal is attenuated at a much faster rate.

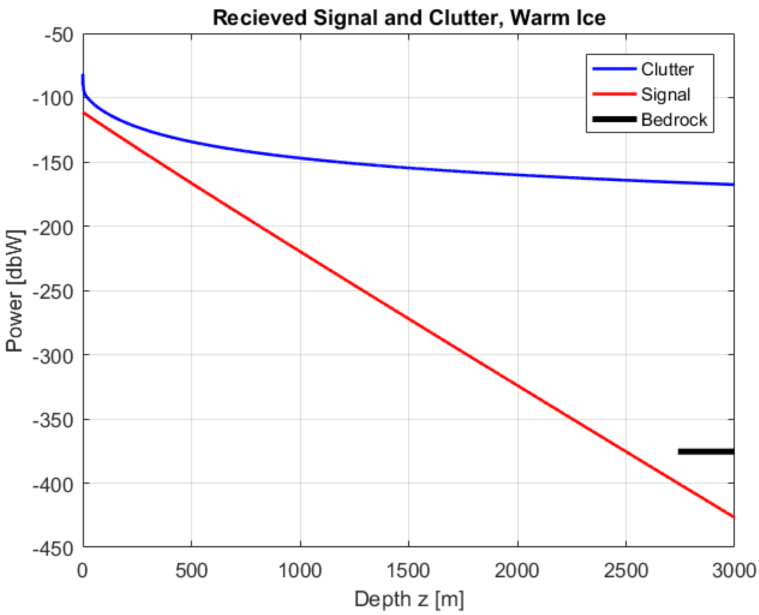

Figure 3.8: Rough surface: Clutter and bed return for warm ice.

The signal is masked by the clutter returns throughout the ice. And by assuming this constant attenuation, the demand would be too high for the filter. To detect bedrock at 3000 meters, the surface clutter should be suppressed approximately 250 dB, and even more with the inclusion of thermal noise.

3.4.2 Recieved power for smooth surface

In contrary to the rough surface, the smooth surface has a very low backscatter, because it is a specular reflection. The clutter returns corresponding to a depth z is therefore much weaker than the backscatter for a rough surface. This is seen in figure 3.9. The signal return from nadir is throughout the ice stronger than the clutter returns. Only in the near surface layers, the clutter is masking the signal of interest. This nevertheless only corresponds to a maximum depth of $z \approx 2m$.

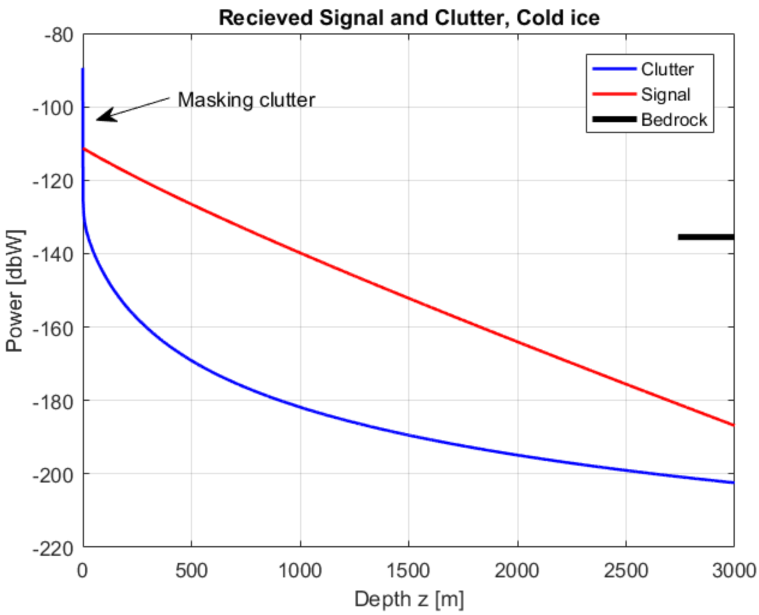

Figure 3.9: Smooth surface: Returns for cold ice.

When the nadir signal is recieved from the deeper layers, the noise could mask the signal when taking the thermal noise into account. And even higher temperatures near the bedrock can contribute to greater attenuation of the nadir signal. Even the geographical location of the radar can play a role, since areas near the water would be warmer than areas in the middle of the ice. However the important intrepetation to be made here, is that the signal level is higher than the clutter level.

In the case of a smooth surface and warm ice, the story is another. The scenario is modelled and seen in figure 3.10. The signal attenuation is now much higher, and it is once again seen that the clutter masks the signal in the first few meters of penetration. Hereafter to a depth z of around 500 meters the signal to clutter ratio is positive and the first frequency band can be weighted less that the additional bands. However the rest of the frequency bands require a good filtration. To detect bedrock the clutter in the last frequency band should be supressed with atleast 200 dB. (Without taking thermal noise into account).

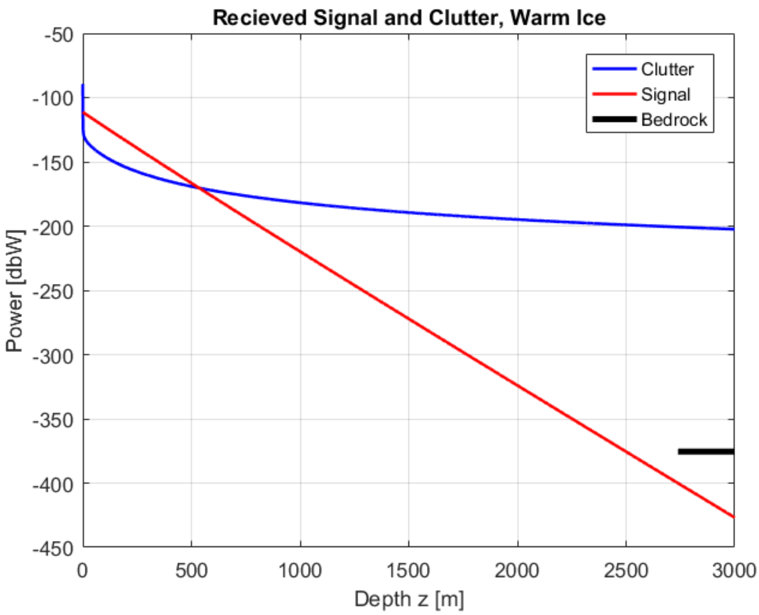

Figure 3.10: Smooth surface: Returns for warm ice.

With the scenarios with cold and warm ice modelled, the filtration and decimation is now performed and the final filter design choices are then presented in the following chapter.

CHAPTER 4

Results and comparisons

This chapter presents the achieved results. This involves suppression of surface clutter for 4 design cases. The filters are designed for the specific scenarios:

- Rough surface and signal attenuation in cold ice $\alpha = 2\ dB/100m$
- Rough surface and signal attenuation in warm ice $\alpha = 10\ dB/100m$
- Smooth surface and signal attenuation in cold ice
- Smooth surface and signal attenuation in warm ice

To evaluate the performance of the filters, mean signal-to-clutter ratios are calculated and presented throughout the chapter, and summarized in the end of the chapter.

4.1 The rough ice surface

In this section the final filter designs are presented for the rough ice surface. This involves the scenarios for cold ice, where the signal attenuation is small, and for the warm ice, where the signal attenuation is high.

4.1.1 Filter design for cold ice

Considering the recieved clutter and signal, seen in figure 3.7, it is desired to supress the recieved clutter to obtain a good signal-to-clutter ratio. The following plot illustrates the filtration of the clutter, with unity weights in the FIRPM weight-vector.

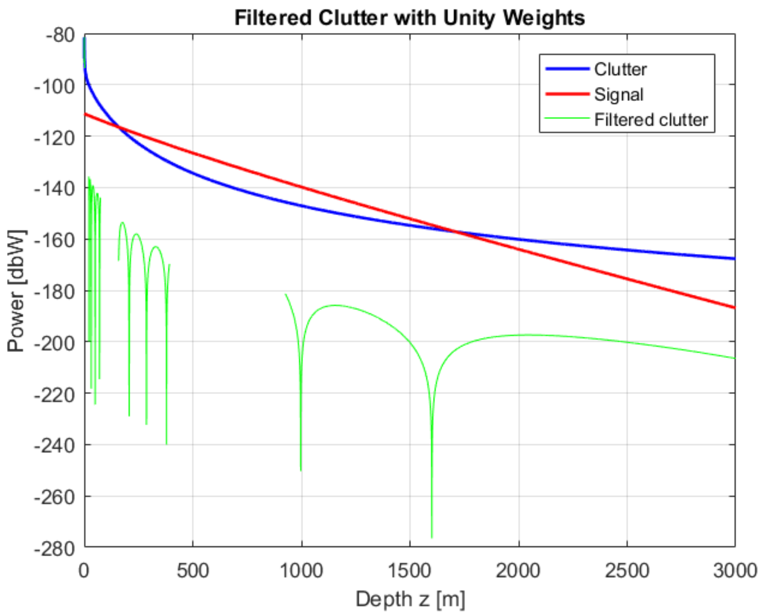

Figure 4.1: Filtered with unity weights.

As previosuly mentioned the use of no weighting function (w=1) results in a stopband attenuation of -35 dB in every band. This is clearly seen from the filtered clutter return. It is suppressed by -35 dB. Because the returns are plotted against the depth z, the filtered clutter gets stretched as seen from the figure. And again the attenuation should be considered as the envelope of the filtered clutter. The signal to clutter ratio is found by comparing the total power of the filtered clutter with the total signal power. The signal-to-clutter ratio with no weighting is

$$SCR = 25.39\ dB$$

This is certainly good, but can be further improved. However the weighting should be performed with caution. Weighting specific frequency bands much more than other bands, will challenge the performance of the filter. For example weighting the three frequency bands 100 times more than the additional bands will result in a stopband attenuation of -20 dB in the additional bands, which is very little. Even though weighting is not neccesarry (suppressing more than 35 dB), the weighting is still performed to achieve a better signal-to-clutter ratio. The actual filter is shown in figure 4.2

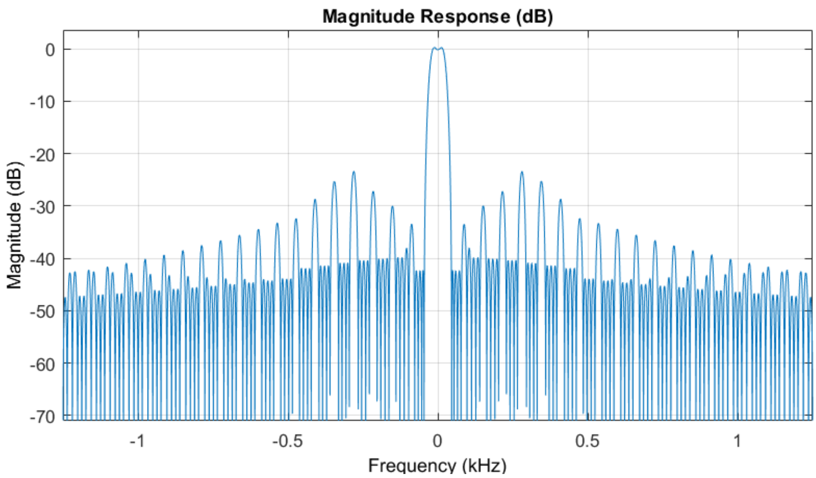

Figure 4.2: Weighted filter: Rough surface and cold ice.

Even though the implementation only concerns the surface clutter, the additional bands are also weighted to ensure proper supressions in those bands. The generated filter coefficients can be found in the Matlab file filtercoeff.m. The passband is weighted with $w = 10$ to make sure that no signal amplification occur in the passband. This passband weighting significantly affects the signal-to-clutter ratio, and should be set to a minimum, while still achieving zero gain in the passband. The mean signal-to-clutter ratio improves to

$$SCR = 32.0032 \ dB$$

4.1.2 Filter design for warm ice

As presented in the implementation a very large suppression is required when considering the warm ice. The green curve illustrates the first three bands after filtration with unity weights, and the black curve is with weights. For both cases with weights and without the SCR is positive for the first internal layers down to a depth of approximately 400 meters. In the deeper layers the clutter is masking the signal. With the use of extreme weights

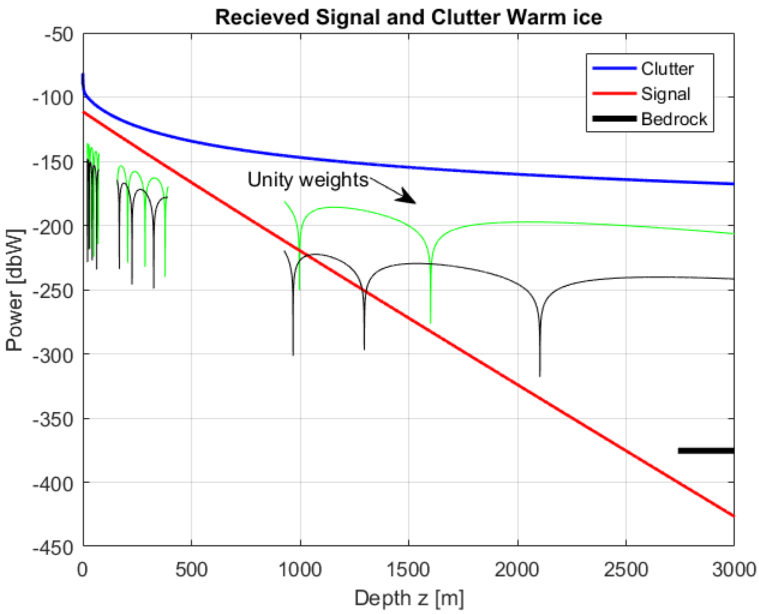

Figure 4.3: With and without weights.

By the use of extreme weights, the mean SCR is improved to $SCR = 9.86\ dB$, which however is not representive for the deeper layers, but is rather included to assess the overall mean performance. The filter coefficients are found in filtercoeff.m.

4.2 The smooth ice surface

4.2.1 Filter design for cold ice

For the smooth ice surface with a cold ice scenario, it was found that the signal return was significantly stronger than the corresponding clutter returns. It is therefore chosen to filter with unity weights. The magnitude response of the filter is seen in figure 4.4

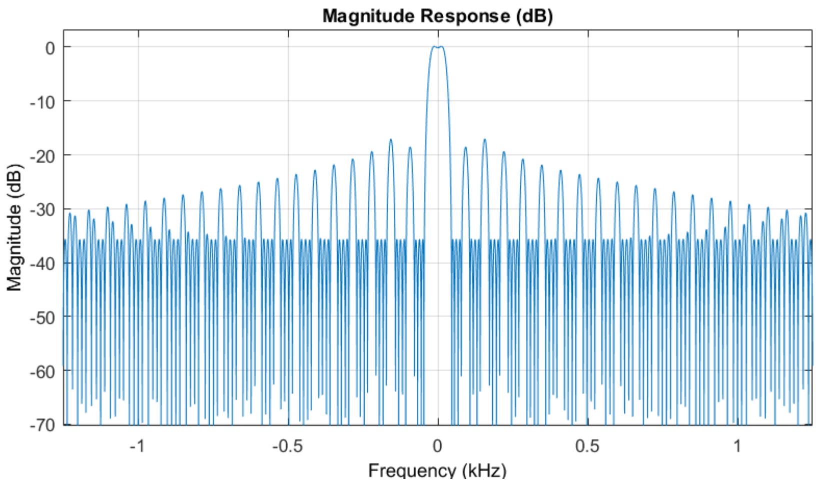

Figure 4.4: Smooth surface and cold ice filter.

With unity weights, the attenuation throughout every frequency band is the same constant of $\approx -35\ dB$. The mean SCR is

$$SCR = 60.13\ dB$$

4.2.2 Filter design for warm ice

As seen from the implementation in figure 3.10 filtering is needed to acheive a better SCR after around 500 meters. By filtering this distance is improved to 1330 meters, and herefter the signal to clutter ratio is very poor. In figure 4.5 the magnitude response is shown.

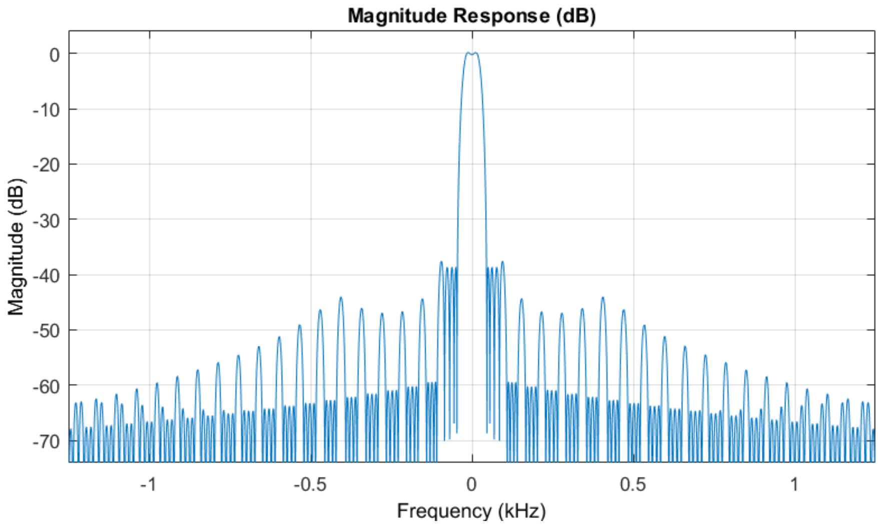

Figure 4.5: Smooth surface and warm ice filter.

The attenuation in the first band is not as important as for the rest of the frequency bands. A mean SCR is again calculated, but it should be noted that the ice is still masked by clutter after roughly 1330 meters.

$$SCR = 35.22\ dB$$

4.3 Summary of results

This section briefly summarizes the achieved results for the different design cases, and the mean signal-to-clutter ratios are compared. In table 4.1 the mean signal-to-clutter ratios are listed.

Table 4.1: Mean SCR values.

Scenario	Mean SCR
Rough surface cold ice	32.03 dB
Rough surface warm ice	9.86 dB
Smooth surface cold ice	60.13 dB
Smooth surface warm ice	35.22 dB

The table gives an overview of the very generalized performance. In the situations where the ice is assumed warm the signal is masked by the surface clutter after roughly 1000 meters and 1330 meters for the rough and smooth surfaces respectively. But for the cold ice scenarios the clutter can effectively be suppressed a great ammount below the corresponding signal levels. And it is in general only masking the near surface layers. For the rough ice with a cold signal attenuation it was found that that the signal would be masked for deeper layers > 1700 meters, and thereby a suppression in this region is essential. Because of the powerful bedrock return, the bedrock would in this case always remain clearly visible.

Another important issue to notice is that the passband should be weighted, which leads to a more analytical tradeoff approach when deciding the weights of the additional frequency bands, and comparing the SCR. The chosen weighting values are given in the filtercoeff.m file, and can be run to achieve the same results as presented.

CHAPTER 5

Program architecture and user manual

The purpose of this chapter is to present the architecture of the written software in Matlab. First a block diagram of the program architecture is given, and then the functionality of the different programs are briefly explained. Figure 5.1 shows the architecture of the program

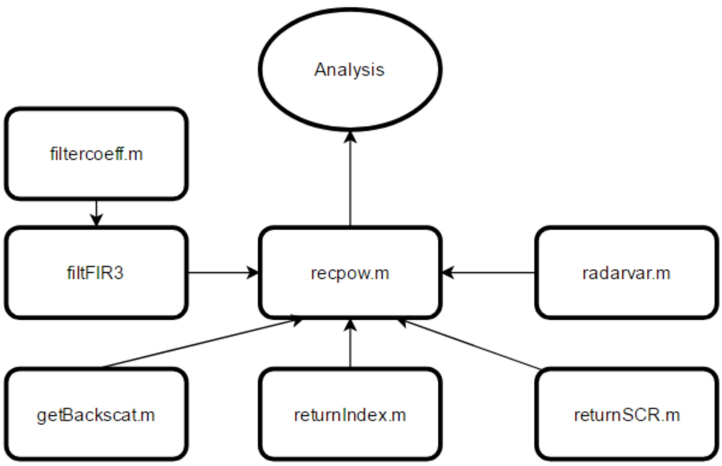

Figure 5.1: Program architecture.

recpow.m is the main program where everything is run from, and which outputs the recieved power and plots. The additional programs are either functions or matlab script files. Only getBackscat.m and returnIndex.m are matlab functions, the additional scripts are called within eachother with the integrated ”run” command.

5.1 radvar.m

radvar.m contains the static variables that should not be changed, with one exception. The file contains parameters like the height of flight, speed of light and static radar variables. Furthermore the file contains the incident angle vector defined until 89 degrees, the depth z expressed as a function of incident angle, and the doppler frequency which depends on the incidient angle. The exception is the attenuation in the ice, which is currently set to 2 dB/100m. If needed this value should be changed in this file.

5.2 recpow.m

This script calculated the power return for a scenario and plots it. The main calculations are performed in this file. This involves the complete implementation of the radar equation.

5.3 filtercoeff.m

In this script the firpm filter is created. This is done in a for loop with 40 iterations, defining each frequency band. Outside the for loop, the amplitude vector is defined. The band weighting must be specified in this file. It is currently set to unity weights, but the script contains the weights for the design cases (commented).

5.4 filtFIR3

This file runs the filter coefficients in the first line. The script then calculates the filtration and decimation in the frequency domain. Only the positive half spectrum is worked with because of the symmetry. To give an overview of the functionality following steps are performed:

1. Steps

    a) Define frequency vector

    b) Define filter spectrum by fft operation, which is interpolated

    c) Split spectrum in half

    d) Define signal to be filtered from recpow.m

    e) Perform frequency domain filtration

    f) Decimation picks out every stopband in the defined frequency range

5.5 getBackscat.m

This function is called within the main program "recpow.m". From the recpow.m the getBackscat argument should be set. When the input argument back = 0 the function returns the backscatter for a smooth surface. When the input argument is back = 1, the function returns the backscatter vector for the rough surface. How the function works is explained below

1. Steps
   a) Load backscatter diagram
   b) Make linear regression from the values
   c) Implemententing the extrapolation assumptions

For the rough surface it is assumed that the backscatter is constant after 6 degrees. And for the smooth surface it is assumed that backscatter is constant after 4.3 degrees.

5.6 returnSCR.m

This function returns the mean signal-to-clutter ratio for the first three bands. The input argument is the decimated clutter and the signal. The function calculates the power in the frequency bands of interest, which leads to zeros in the vector because of the transition bands. The zeros are removed and the mean power is calculated. The output is "SCR".

5.7 returnIndex.m

This function is used throughout the program. When it is desired to know the index of a specific doppler frequency or a specific depth z in the ice. The function can take two string values as input. Below an example is given

1. index = returIndex('zdep',1000)
2. index = returnIndex('fd',62.5)

The output is then the index corresponding to either a depth in the ice of 1000 meters, or the index of the doppler frequency corresponding to 62.5 Hz

5.8 External

The script "sincfilt.m" was written in the intial stages of the project, and is used to calculate the SNR improvement of the filtering process for the integrate and dump filter. Therefore it is not included as a part of the main programs.

Furthermore the antenna diagram for the along track and the backscatter values must be inside the root folder, for the program to run. These files are attatched in a zip file along with the other programs.

CHAPTER 6

Conclusion

In the intital stages of the project it was found that the equiripple finite impulse response filter, was the most suitable filter for the design cases. The filter design method is implemented with Parks-McClellan optimal filter design algorithm (firpm in Matlab). With the project based around the nadir looking radar POLARIS, a lot of new radar theory has been studied. This involves a complete simulation of the recieved power returns from the nadir signal, and the surface clutter returns. By the use of empirical backscatter data, the inclusion of the real along-track antenna diagram, and the radar parameters the radar system was successfully modelled. Several routines were written in Matlab, which alltogether formed the complete program.

By modelling the power returns it was seen how several parameters significantly changed the need for clutter suppression. When considering the ice as warm for the signal propagation, the corresponding clutter returns recieved at same time instantses is much more powerful, and the clutter therefore masks the signal of interest. In these scenarios, the attenuation demand is too high for the filter, and the visisibility for warm ice is therefore limitted. On the contrary for the cold ice, the need for clutter supression is smaller, and the bedrock can easiliy be detected. The final results are visually interpreted, through the several plots in chapter 5. Mean signal-to-clutter values are however also presented, but they are of less meaning in the cases for time instances with negative SCR, since a good average SCR doesn't mean that the SCR is good everywhere.

By the comprehensive study of radar theory, applying digital signal processing and using filter theory, several filters were designed to suppress the surface clutter returns.

6.1 Future work

In the final designs the thermal noise was not accounted for. This was due to a wrong implementation (not taking the pulse compression gain into account). Unfortunately a lack of time resulted in neglecting the thermal noise. The thermal noise should definately be implemented as a part of the future work in this project. With slight modifications in the program the thermal noise can be included. Another aspect that should be shed light on, would be to asses the effect of quantization noise present, and implementing it in the program.

In the scope of the project only the nadir looking radar was worked with, another interesting case to implement would be the side looking radar. This would not involve too much work, and could be handled by the inclusion of the cross track antenna diagram, and hereby representing the full radiation pattern.

Bibliography

[1] T Parks and J McClellan. "Chebyshev Approximation for Nonrecursive Digital Filters with Linear Phase". In: *IEEE Transactions on Circuit Theory* 19.2 (1972), page 192.

[2] John G. Proakis and Dimitris G. Manolakis. "Digital Signal Processing". In: *Digital Signal Processing*. 1996, pages 661–662.

[3] Anders Kusk and Jacob Mohr. "SAR Light - an Introduction to Synthetic Aperture Radar". In: *DTU material* (2006), pages 36, 7.

[4] John G. Proakis and Dimitris G. Manolakis. "Digital Signal Processing". In: *Digital Signal Processing, Principles, Algorithms, and Applications, Fourth Edition*. 2007, page 385.

[5] Merrill I. Skolnik. *Introduction to Radar Systems*. Volume 1081. 2009, page 33. ISBN: 0070579091. DOI: 10.1017/CBO9780511608117.001. arXiv: 0712.0689.

[6] J. Dall et al. "ESA'S POLarimetric Airborne Radar Ice Sounder (POLARIS): design and first results". In: *IET Radar, Sonar & Navigation* 4.3 (2010), page 488.

[7] Ulrik Nielsen. "Ice sounding". In: *DTU study material for 30340 Radar Radiometer Systems* (2014), 11–15 POLARIS key parameters on P.24.

[8] Ulrik Nielsen. "Ice sounding". In: *DTU study material for 30340 Radar Radiometer Systems* (2014), Formulas: 2.20, 2.23, 2.24.

[9] Jørgen Dall. Personal communication. 2017.

[10] *Figures*. [Self made figure either in LateX using "Tikz" package or in MATLAB]. 2017.

[11] *Parks-McClellan optimal FIR filter design*. https://se.mathworks.com/help/signal/ref/firpm.htm MATLAB.

*Picture on front page is obtained from [9]7

DTU Space
National Space Institute
Technical University of Denmark

Elektrovej, building 327
DK - 2800 Kgs. Lyngby
Tel (+45) 4525 9500
Fax (+45) 4525 9575

www.space.dtu.dk